nature astronomy

LETTERS

DOI: 10.1038/s41550-017-0238-6

Polarization due to rotational distortion in the bright star Regulus

Daniel V. Cotton[1*], Jeremy Bailey[1], Ian D. Howarth[2], Kimberly Bott[3,4], Lucyna Kedziora-Chudczer[1], P. W. Lucas[5] and J. H. Hough[5]

Polarization in stars was first predicted by Chandrasekhar[1], who calculated a substantial linear polarization at the stellar limb for a pure electron-scattering atmosphere. This polarization will average to zero when integrated over a spherical star but could be detected if the symmetry was broken, for example, by the eclipse of a binary companion. Nearly 50 years ago, Harrington and Collins[2] modelled another way of breaking the symmetry and producing net polarization—the distortion of a rapidly rotating hot star. Here we report the first detection of this effect. Observations of the linear polarization of Regulus, with two different high-precision polarimeters, range from +42 ppm at a wavelength of 741 nm to −22 ppm at 395 nm. The reversal from red to blue is a distinctive feature of rotation-induced polarization. Using a new set of models for the polarization of rapidly rotating stars, we find that Regulus is rotating at $96.5^{+0.6}_{-0.8}$% of its critical angular velocity for break-up, and has an inclination greater than 76.5°. The rotation axis of the star is at a position angle of 79.5 ± 0.7°. The conclusions are independent of, but in good agreement with, the results of previously published interferometric observations of Regulus[3]. The accurate measurement of rotation in early-type stars is important for understanding their stellar environments[4] and the course of their evolution[5].

Initial efforts to detect Chandrasekhar's polarization effect proved unsuccessful, leading instead to the discovery of interstellar polarization[6,7]. The predicted polarization in an eclipsing binary has been observed only once, in Algol[8]. The early models of these effects used pure electron scattering atmospheres[1,6]. When more realistic non-grey stellar-atmosphere models were applied to rotating stars[9,10], the expected polarization at visible wavelengths was found to be much smaller. Indeed, the low predicted polarizations were used to infer that this mechanism could not explain the large polarizations observed[11] in Be stars, which are now attributed to circumstellar decretion disks[12,13].

The development, over the past decade or so, of a new generation of polarimeters[14–16] that can measure stellar polarization at the ppm level brings the small atmospheric polarization effects into the range of observations. Using one of these instruments, PlanetPol[15] on the 4.2-m William Herschel Telescope, the polarization of Regulus was measured[17] as 36.7 ± 0.8 ppm, which stood out from the much smaller polarizations measured for other stars at similar distance in the same part of the sky. It was concluded that the polarization was likely to be intrinsic. As Regulus is a rapidly rotating star, polarization due to rotational distortion was considered a possibility. Models had previously been calculated[10] for rapidly rotating stars of types B0, B1, B2 and B5, and extrapolation of these to Regulus' B7V spectral type suggested that the polarization was about what was expected for a star rotating at 95% of the critical angular velocity for break-up, very similar to the rotation rate determined from interferometric observations at the time[5]. However, as only one wavelength was observed, further observations and modelling were needed to confirm the interpretation.

Here we combine the PlanetPol observations with new observations of Regulus obtained with the High Precision Polarimetric Instrument, HIPPI[14], on the 3.9-m Anglo-Australian Telescope at Siding Spring Observatory. These observations were made in four broad wavelength bands with effective wavelengths of 393, 461, 597 and 618 nm. The PlanetPol observations are in a redder band with an effective wavelength of 741 nm. In Fig. 1 we show the measured polarizations, averaging all observations in each band and correcting for a small amount of interstellar polarization (see Methods). The data are plotted in the form of a Q–U diagram, where the normalized Stokes parameters Q/I and U/I are related to the degree of polarization p and position angle θ (measured eastwards from north) through $Q/I = p\cos 2\theta$ and $U/I = p\sin 2\theta$.

It can be seen from Fig. 1 that the polarization varies strongly with wavelength, and the points lie nearly on a line passing through the diagram's origin. This is exactly what is expected for polarization due to rotational distortion, where gravity darkening toward the equator induces a wavelength-dependent asymmetry in the stellar disk. The Sonneborn models[10] show just this reversal of direction with the polarization being parallel to the star's rotation axis at red wavelengths, and perpendicular to the star's rotation axis in the ultraviolet (when the coordinate system is rotated to align Stokes Q with the star's rotation axis, this corresponds to positive and negative polarization respectively, and we present data by this convention later). In the Sonneborn B5 model[10], the reversal of polarization occurs at ~380 nm. In our Regulus observations, it occurs at ~480 nm. However, this is entirely consistent with the trend shown in the Sonneborn models[10] of the reversal shifting to longer wavelengths for later-type stars.

Several factors give us confidence in the reliability of the observations. All wavelength bands have been observed multiple times. The repeat observations agree very well even with observations separated by months to years (see Methods). There is no indication of any variability. We can exclude the possibility of Regulus' companion significantly affecting our measurements

[1]School of Physics, University of New South Wales, Sydney, New South Wales 2052, Australia. [2]Department of Physics and Astronomy, University College London, Gower Street, London WC1E 6BT, UK. [3]Virtual Planetary Laboratory, Seattle, WA 98195, USA. [4]Astronomy Department, University of Washington, Box 351580, Seattle, WA 98195, USA. [5]Centre for Astrophysics Research, School of Physics, Astronomy and Mathematics, University of Hertfordshire, Hatfield AL10 9AB, UK. *e-mail: d.cotton@unsw.edu.au

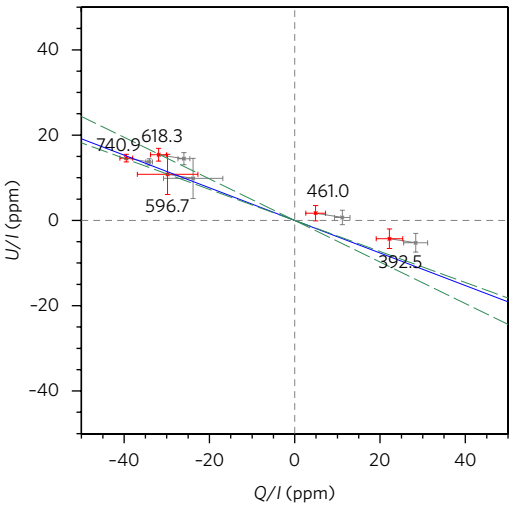

Fig. 1 | Polarization observations of Regulus on a *Q*–*U* diagram. Polarization observations of Regulus averaged for each band (grey points) and the same observations corrected for interstellar polarization (red points). Error bars (1σ) for the observations are derived from the internal measurement statistics and those of the telescope polarization; the interstellar corrected points also include a contribution derived from the scatter in interstellar polarization measured in nearby stars. Labels show effective wavelength in nanometres. The blue line is the fitted orientation for the rotation axis of the star (see Methods). The green dashed lines show the bounds on the rotation axis of the star as determined by interferometry[3].

(see Supplementary Information). The observations obtained with the two different instruments are very consistent, with polarization (after correction for interstellar polarization) in HIPPI's reddest band being $p = 35.4 \pm 1.6$ ppm at $\theta = 77.1 \pm 1.3°$, and that measured by PlanetPol being $p = 42.1 \pm 1.2$ ppm at $\theta = 79.9 \pm 0.7°$. The increase in p with wavelength is as expected, and the position angles are very similar. These data were obtained 10 years apart, those with PlanetPol in 2005–06, and those with HIPPI in 2016. We have observed several stars at similar distances and in the same region of the sky with both instruments, and none shows polarizations nearly as high as those seen in Regulus. Furthermore, when we fit the position angle of the polarization by minimizing U/I (see Methods), it aligns well with the rotational axis of Regulus as determined by interferometry[3], shown with green dashed lines in Fig. 1.

To provide further confirmation of the mechanism of polarization and to allow constraints on the properties of the star, we have developed a new set of models for the polarization of rotating stars, verifying the code by comparison with the model results of ref. [18] and ref. [10] (see Methods).

Each model uses as a starting point a value for the angular velocity expressed as ω/ω_c, where ω_c is the critical angular velocity for break-up of the star. Given this and a chosen value for the effective temperature (T_p) and gravity (g_p) at the pole, we can calculate the distribution of local effective temperature, $T_{\rm eff}^{\rm l}$, and g over the star. The effective gravity g is a function of the colatitude Θ and can be determined by methods described in the literature[2,9]. The variation of $T_{\rm eff}^{\rm l}$ with colatitude depends on adopting a gravity-darkening law. For our Regulus models we use the ELR gravity-darkening law[19]. This law has been developed specifically for rapidly rotating stars and provides results that agree well with two-dimensional models of rotating stars as well as with interferometric observations, which show generally less variation of $T_{\rm eff}^{\rm l}$ over the stellar surface than predicted by the classic von Zeipel law[20].

We then create a set of 46 ATLAS9[21] stellar-atmosphere models each calculated for the pair of $T_{\rm eff}^{\rm l}$ and log g values that apply at colatitudes from 0 to 90° with 2° intervals. We calculate the emergent specific intensity (radiance) and polarization as a function of μ (cosine of the viewing zenith angle) and wavelength for each of these models with a version of the SYNSPEC spectral-synthesis code[22] that we have modified to do radiative transfer with full polarization using the Vector Linearized Discrete Ordinate (VLIDORT) code from RT Solutions[23].

We then select an inclination at which to view the star, and set up a grid of 'pixels' covering the observed view, spaced at intervals of 0.01 of the polar radius. For each pixel that overlaps the star, we calculate the colatitude Θ and viewing angle μ. We can then interpolate in our grid of 46 models and 21 μ-values to obtain the specific intensity and polarization for that pixel. These can then be plotted to create images such as those in Fig. 2 for a specific wavelength range, or integrated across the star to provide the flux and polarization spectrum at high resolution.

The polarization wavelength dependence is a complex combination of effects arising from the change in polarization as a function of μ (see, for example, Supplementary Fig. 4) and the change in relative contributions of equatorial and polar regions at different wavelengths (for example Fig. 2) and temperatures according primarily to the Planck function[9]. Figure 3 shows how the modelled parameters affect the polarization wavelength dependence. All four main parameters are significant. Increasing T_p shifts the whole curve upwards, and therefore shifts the crossover from negative to positive polarization to shorter wavelengths. Decreasing the inclination reduces the positive polarization at red wavelengths while having little effect on the negative polarization in the blue. Increasing ω/ω_c or decreasing log g_p increases all polarization, making the red polarization more positive, and the blue more negative. As a result, the effects of ω/ω_c and gravity cannot be readily distinguished.

It is not, therefore, possible to uniquely determine all four parameters from polarization data alone. To progress further, we need additional constraints. Using an inversion of the method for finding distance described in ref. [24], we can use the known distance and hence absolute magnitude ($M_V = -0.58$) and spectroscopically determined projected equatorial rotational velocity, $v \sin i$, for which we use 318 ± 8 km s^{-1} (see Methods), to derive the global effective temperature, $T_{\rm eff}$ (and hence T_p) and log g_p, given values of ω/ω_c and i. This provides a two-dimensional parameter space which we have explored by calculating a grid of models, in the range $\omega/\omega_c = 0.9$ to 0.99 and $i = 65$ to 90°; Fig. 4 shows the results of fitting these models to our data.

From Fig. 4, and after additionally taking account of errors in $v \sin i$ and $F_{\rm UV}$ (see Methods), we obtain $\omega/\omega_c = 0.965^{+0.006}_{-0.008}$ and $i > 76.5°$ with a best-fit value of 80.0°, which corresponds to $T_p = 14,375^{+215}_{-181}$, and $\log g_p = 3.992^{+0.022}_{-0.026}$. The results are in excellent agreement with interferometry[3] in which results of $\omega/\omega_c = 0.962^{+0.013}_{-0.028}$ and $i = 86.3^{+1.7}_{-2.3}$ degrees were obtained. The bottom left panel of Fig. 3 shows that polarization is particularly sensitive to ω/ω_c near critical velocity; consequently we are able to constrain ω/ω_c more tightly than by interferometry. Our determination of inclination is not as precise as that from interferometry. It can be seen from the bottom right panel of Fig. 3 that the models are not very sensitive to inclination near 90°. This difficulty would not be encountered if the star were less inclined; in the present instance, it might be overcome by high-precision spectropolarimetry. Although U/I is negligible across the broad band, our models show polarizations in spectral lines owing to the Öhman effect[25] (see Supplementary Information). This polarization is zero at 90° and increases rapidly with decreasing inclination.

Particularly in extreme stars, such parameters as we have determined here are of great importance. They are needed, for instance, to track the star's evolutionary path accurately along the Hertzsprung–Russell diagram[5] and therefore determine its end

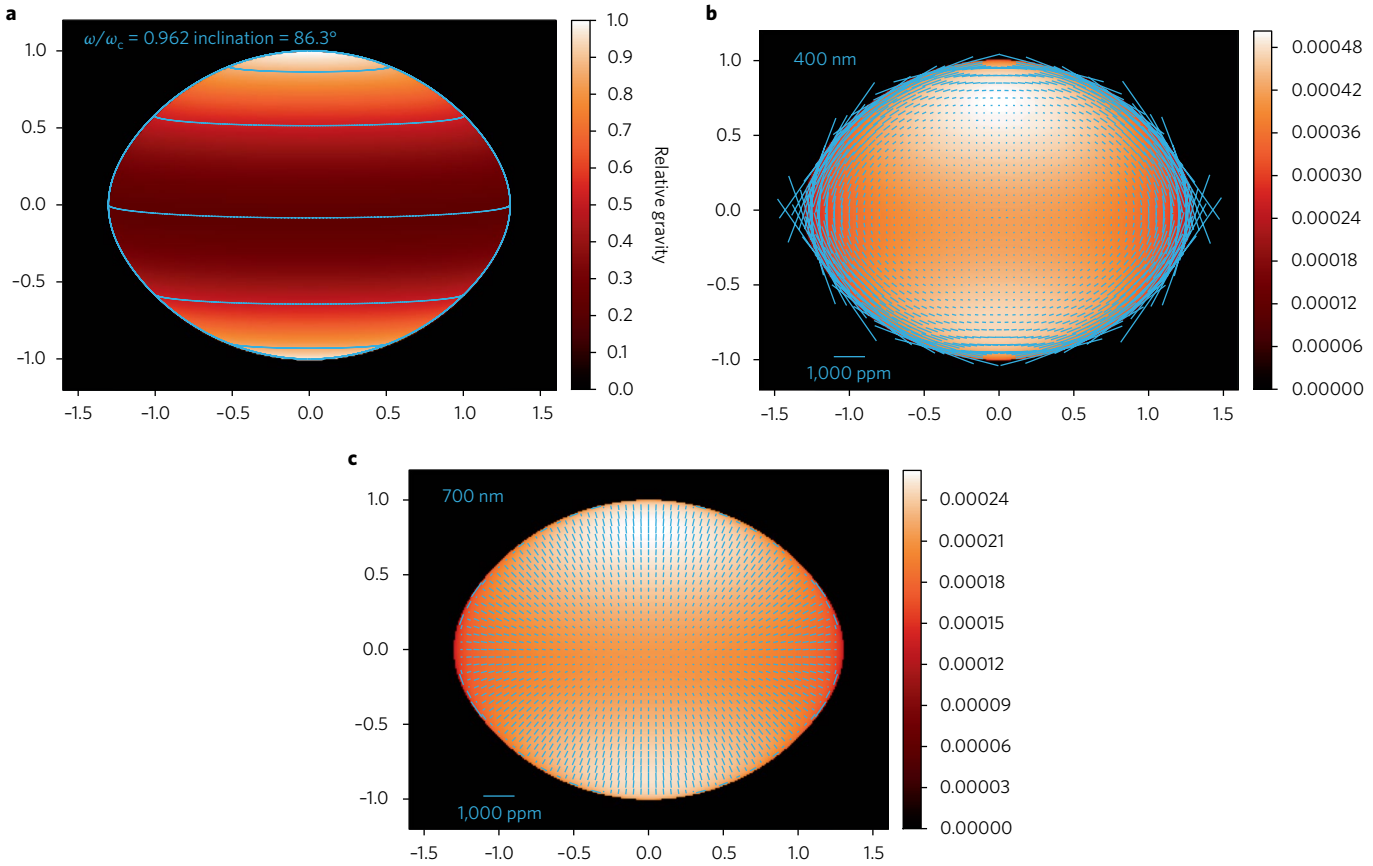

Fig. 2 | Example of polarization modelling of Regulus. a, Distribution of effective gravity over the surface of the star, in this case for $\omega/\omega_c = 0.962$ and inclination $i = 86.3°$ (the interferometry parameters determined in ref. [3]). **b**,**c**, Derived intensity distribution over-plotted with polarization vectors at wavelengths of 400 nm and 700 nm, respectively. The intensity scale is specific intensity (or radiance) I_ν in units of erg cm^{-2} s^{-1} Hz^{-1} sr^{-1}.

state (for example supernova or compact remnant), or to determine the limits of the Be phenomenon. Rotation also affects how much mass is lost back into the interstellar medium and the local space weather in the form of stellar winds[4]. Yet, so far, only half a dozen rapidly rotating stars have been resolved with interferometry, whereas our initial estimates indicate that we may be able to determine parameters for three times that number with our present instrumentation and facilities. This result thus represents considerable progress for stellar linear polarimetry. Previously, the field has been largely restricted to studying material external to stars or those with extreme magnetic fields[12]. Now we are able to probe fundamental parameters of the stellar atmosphere itself.

Methods

Multi-band high-precision polarimetry. We made observations with two high-precision polarimeters: PlanetPol[15] and HIPPI[14]. High-precision polarimetry requires the use of high-frequency modulation to eliminate the effects of astronomical seeing. PlanetPol uses photoelastic modulators oscillating at tens of thousands of hertz. HIPPI uses ferroelectric liquid crystal technology to provide modulation at 500 Hz.

The PlanetPol observations were made in a single broad red band that runs from 575 to 1,025 nm. With HIPPI we used three different filters, those being a 425-nm short-pass filter (425SP), and Sloan Digital Sky Survey g′ and r′ filters. All three filters were used in combination with the blue-sensitive Hamamatsu H10720-210 ultra bi-alkali photocathode photomultiplier tube (PMT) (b). We also made observations with the r′ filter paired with the red-sensitive Hamamatsu H10720-20 infrared-extended multi-alkali photocathode PMT (r), resulting in five bands in total.

Because of the filter and PMT profiles, and the modulator performance, the effective wavelength and polarization efficiency vary with the spectral type of the target. We have calculated these for each band using the bandpass model described in ref. [14]. Some, but not all, of these have been reported previously[14,26,27], so for completeness we list the bandpass calculations for each filter/PMT combination used here in Supplementary Table 1, along with the corresponding PlanetPol bandpass calculations[15]. The stars that we observed for this work—Regulus and various calibration standards—are within 60 pc, so no interstellar reddening has been applied in the bandpass model. We have also made bandpass calculations specifically for Regulus. The stellar model used for this is amongst the suite of models described in the Polarization Radiative Transfer section; specifically, it is the one with $\omega/\omega_c = 0.95$ and $i = 90°$. The various band sensitivities and effective wavelengths as applied to the Regulus stellar model are shown in Supplementary Fig. 1.

The r′(b) observations in May 2014 used a different modulator from all the other HIPPI observations. This gave a 1.5% higher efficiency than the data in Supplementary Table 1 (see notes in the table).

Observations and calibration. The PlanetPol observations, taken in April 2005 and February 2006 at the 4.2-m William Herschel Telescope in La Palma, have been detailed previously[17]. There the standard A0 efficiency correction from Supplementary Table 1 was applied[17]. Here we have instead applied a bandpass model specific to Regulus, and error-weighted the two observations; the details are otherwise unchanged.

The HIPPI observations were acquired in four observing runs over three years, on the Anglo-Australian Telescope (AAT) at Siding Spring in Australia and are reported here for the first time. For each observation we took measurements at four different position angles of the AAT's Cassegrain rotator (0°, 45°, 90° and 135°). The effects of the background sky are typically removed through the subtraction of a sky measurement, obtained at a separation of 2 arcmin for each PA setting and for each observation. The duration of the sky measurements was 3 minutes per Stokes parameter. The observing, calibration and data-reduction methods are described in full detail elsewhere[14].

Observations of high-polarization standards ($p \approx 1$–5%) were used to calibrate position angle. A list of the high-polarization standards observed (in the g′ band but occasionally checked against similar measurements in other bands) is given in Supplementary Table 2. The precision of each determination is taken to be ±0.5°, based on the mean consistency of the calibration provided by the different reference stars, which themselves have uncertainties of this order.

We use observations of stars previously measured with negligible polarizations to determine the zero-point or telescope polarization. Deviations from zero

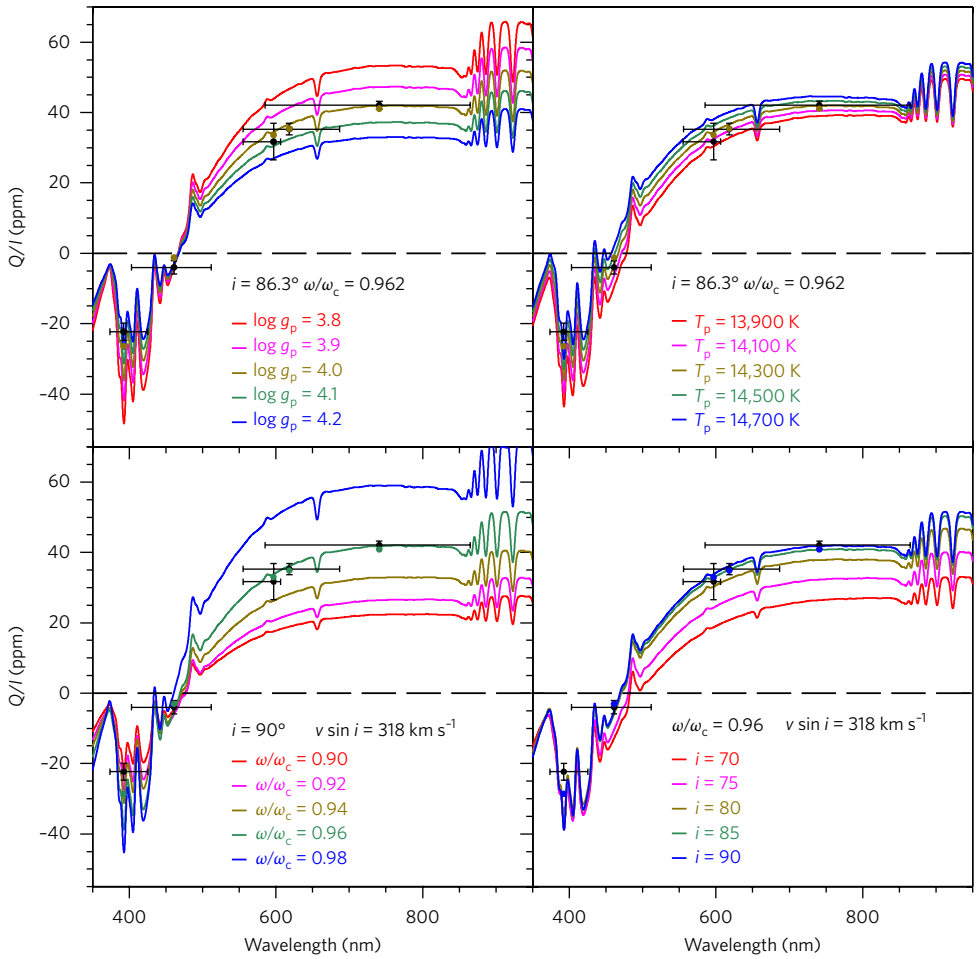

Fig. 3 | Observations of Regulus versus model results. Observations of Regulus (black points with error bars) are compared with smoothed model results showing the effect of varying different parameters (polar gravity, polar temperature, rotation and inclination). The observations have been rotated into the plane of the rotational axis determined for Regulus (that is, by 79.5°), and the error bars show both the formal error in Q/I (as per Fig. 1) and the full-width at half-maximum of the spectral bands. Solid coloured circles show the best-fit model averaged over the observed bandpass. The upper two model sets use the interferometrically determined parameters $\omega/\omega_c = 0.962$ and inclination $i = 86.3$. The lower two models use parameters for a fixed $v \sin i$ of 318 km s^{-1} as explained in the text.

polarization in the standards chosen can therefore be a source of error. To minimize this complication, we keep a very short list of low-polarization standards, about which we can be most certain. Even so, variance in the low-polarization standards could produce differences up to a few ppm in the assumed telescope zero point between runs. To combat this problem here—where exquisite precision is required—we have assigned each low-polarization standard a non-zero polarization based on the best available data.

The assigned polarization values for each standard star are given in Supplementary Table 3, for each band in which they were observed. The assigned values and associated errors for α Serpentis, β Leonis and β Virginis come from PlanetPol observations[17], and are adjusted for other bands based on the polarimetric colour of the interstellar medium (explained in more detail in the next section). By assuming only interstellar polarization, we can use the method outlined elsewhere[28] to determine values for Sirius and β Hydri; this method is described in full in its application to the interstellar subtraction for Regulus in the next section. Q–U plots made to inter-compare our low-polarization measurements are sparsely populated but seem to corroborate the assignments.

The assigned values are subtracted from each standard measurement, and their uncertainties propagated. The error-weighted mean of the standard measurements is then used to determine the telescope polarization. For the error in telescope polarization, we use the greater of either the root-mean-square propagated errors, or the error-weighted mean of the scatter (standard deviation) in the individual measurements. This methodology has its greatest consequence for the May 2014 observations, as there is a significant difference between measurements of α Ser and β Leo. β Leo hosts a debris disk[29], and although the polarization determined with PlanetPol is suitably small, there may be an intrinsic component resulting in anomalous deviation at shorter wavelengths. Subsequent observations of α Ser suggest that very low-level variability may be present; our data are as yet insufficient to test our suspicions. The May 2014 run is the only one for which α Ser and β Leo were used as standards in this work. In other subsequent work, we have tried to avoid using either of these stars as standards. Given these circumstances, the larger error assigned according to the scatter is appropriate.

The observations of the low-polarization standards, rotated into the Q–U frame and corrected according to their assigned values (from Supplementary Table 3), and the resulting telescope polarization are given in Supplementary Table 4.

Observations of Regulus were made during three different observing runs. The exposure times varied according to target availability, weather and other considerations. The observations lasted approximately half an hour to an hour, with second-stage chopping used to swap the sign of the modulation every 40 to 80 seconds. The observations are detailed in Supplementary Table 5. We also observed HD 99028 as an interstellar control; the details of this, along with the PlanetPol observations, are also given in Supplementary Table 5.

Interstellar polarization subtraction. Within the Local Hot Bubble (LHB), interstellar polarization is small (roughly 0.2–2 ppm pc^{-1}). Yet even at this level, accurate subtraction is crucial to measuring intrinsic polarization induced by rapid rotation. Only recently has sufficient precision been obtained in measurements of stars within the LHB[17,26,28,30] to enable accurate interstellar subtraction in this region.

To determine the contribution to our measurements from interstellar polarization we have, in the first instance, used the same method as in past work[28]. Regulus is north of Galactic latitude $b = +30$. From measurements of around 30 stars, the relationship between the magnitude of polarization and distance for this part of the insterstellar medium, in the g′ band, has been determined, on average, to be[28] $p_i = (0.261 \pm 0.017)d$, where p_i is in ppm and d is in pc. Regulus lies at a distance of 24.3 pc (ref. [31]), which gives $p_i = 6.3 \pm 0.4$ ppm. Because the interstellar

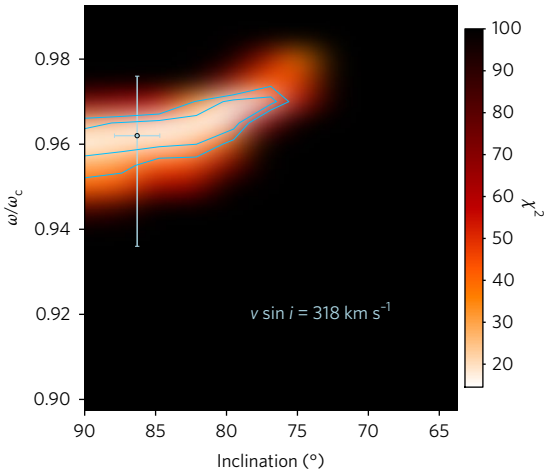

Fig. 4 | Results of model fitting. Results of a grid of models calculated for $v \sin i = 318\,\mathrm{km\,s^{-1}}$ fitted to the polarization observations as a function of wavelength. The resulting χ^2 is plotted as a function of rotation rate and inclination. Models near $\omega/\omega_c = 0.96$ at 90°, 0.965 at 80° or slightly higher values for lower inclinations are the best fits. The contour lines mark the formal 1σ and 2σ uncertainties obtained using a reduced χ^2 statistic. The point with error bars shows the parameters from interferometry and the associated 1σ uncertainty[3].

medium can be clumpy, we have adopted a more conservative estimate of the error in p_i, which we describe below.

Interstellar polarization varies as a function of wavelength. The best current estimate of interstellar polarization colour within 100 pc is described by ref. [27] as likely peaking at 470 nm— having been calculated using the empirically determined Serkowski law[32] as modified in ref. [33]. We have used the relation given there[27] to adjust the magnitude of interstellar polarization in the other bands using their effective wavelengths. The most extreme difference is between the g′ and PlanetPol bands and is ~1 ppm.

In nearby space, it has been shown[28] that the position angles of pairs of stars polarized by the interstellar medium are correlated at angular separations up to 35°, with the correlation being greater at closer separations. In that work, an average of intrinsically unpolarized A–K stars within 50 pc of the Sun, weighted by angular separation, was used to determine interstellar polarizations for nearby FGK dwarfs. Here we use the same approach and list of stars (with the addition of HD 99028) but extend the distance limit to 70 pc from the Sun, as Regulus lies at a greater distance than most of the targets in the earlier study. The control stars from the list with angular separation to Regulus less than 35° are listed in Supplementary Table 6. For each of these stars, we have determined a debiased polarization with distance (where the debiasing is a standard way to account for the effects of measurement error on the positive definite quantity p), and calculated the equivalent polarization at the distance of Regulus. The error-weighted scatter in these measurements from the determined interstellar polarization (6.3 ppm) has been taken as the error in our interstellar determination for Regulus; the adopted value is thus 6.3 ± 1.4 ppm.

The position angles of all the assumed intrinsically unpolarized stars near Regulus are shown in Supplementary Fig. 2. Within 35°, three stars meeting the required criteria were observed with PlanetPol[17], another with HIPPI in the g′ band during a bright-star survey[26], and we have observed one further star with HIPPI in the g′ band; these are listed in Supplementary Table 6. Taking the separation-weighted average of the position angles of these stars gives the interstellar position angle at Regulus as $175 \pm 12°$, where the weight was calculated as $1 - (s/35)$, with s being the angular separation to Regulus in degrees. We assume no angular dispersion with wavelength and we subtract the interstellar polarization at the same angle in every band. Our Regulus observations before and after interstellar subtraction are shown in Supplementary Table 7.

Interstellar reddening. In our bandpass model and in the stellar modelling that follows, we adopt $E_{(B-V)} = 0$. This assumption is justified on the basis of the very low level of interstellar polarization. Within the LHB, photometry is not sensitive enough to accurately measure interstellar reddening[17]. However, past studies have looked at the correlation between $E_{(B-V)}$ and p_i beyond the LHB, and we can use these to infer a likely range for $E_{(B-V)}$ here. A summary of these studies[12] mentions extremes of $p_i/E_{(B-V)} \leq 9.0$ (ref. [32]) and 0.18 (ref. [34]). Although we do not know what the specific relationship is for nearby space, it is reasonable to conclude that $E_{(B-V)}$ is probably much less than 0.005.

Determination of Regulus' rotation-axis position angle. A determination of Regulus' rotation-axis position angle, θ_R, can be made after subtraction of the interstellar polarization from the raw measurements. This is accomplished by assuming that any intrinsic polarization is due to rotational oblateness, and rotating Q/I and U/I into a new reference frame (Q_r/I, U_r/I) that minimizes U_r/I. In practice, we use Python's 'scipy.optimize.curve_fit' routine with its 'trf method' and error-weight each of the bands. This gives θ_R as $79.5 \pm 0.7°$, in good agreement with the interferometric determination[3] of 77 to 80°. The polarization in each band after rotation by this angle is given in Supplementary Table 7.

Determination of projected equatorial rotation velocity. As discussed below, the equatorial rotation velocity of Regulus, $v \sin i$, provides a useful constraint on system parameters. The literature reports a rather wide range of values for the former parameter (~260–350 $\mathrm{km\,s^{-1}}$; for example refs [35,36]), so to make a new determination we de-archived high-resolution spectra obtained with several echelle spectrographs (UVES[37], HARPS[38], FEROS[39] and Elodie[40]; resolving powers $\sim(5–10) \times 10^4$, signal-to-noise ratios ~500 for each instrument in merged datasets). The spectrum of Regulus is dominated by strong hydrogen-Balmer lines (consistent with its spectral type), with the star's rapid rotation leading to blending of other characteristic features (specifically, the He I/Mg II 447.1/448.1-nm classification lines). After examining the spectrum, we chose the isolated, unsaturated Si II 634.7-nm line (Si II λ634.7) for analysis (as in ref. [41]). This is a 'cold' line (its equivalent width increases monotonically going from equator to pole in our models), and continuum gravity darkening is not severe at this wavelength (half of the observed 650-nm continuum flux originates from colatitudes of 70° or greater); consequently Si II λ634.7 does not suffer strongly from the degeneracy between linewidth and equatorial rotation velocity discussed previously[42].

Although direct modelling of the spectral-line profile can yield estimates of $v \sin i$, its Fourier transform encodes this information in a more straightforwardly accessible manner, with the first minimum in the Fourier transform scaling linearly with $v \sin i$ for a spherical star and wavelength-independent limb darkening[43]. However, rotational distortion, gravity darkening and wavelength-dependent limb darkening all modify the scaling factor, and noise can influence the precise location of the minimum. Synthetic spectra were therefore generated for full rotating-star models, using Roche geometry and ATLAS9 model atmospheres as described below, for an appropriate range of $v \sin i$ values. (The results are insensitive to the precise values adopted for other stellar parameters, as we confirmed through sensitivity tests.) The model spectra were convolved with approximate (Gaussian) instrumental profiles; and noise, determined directly from the observations, was added. The Fourier transforms of the observed and model spectra were then compared in order to determine $v \sin i$. The modelling fully accommodates any small residual nonlinearity between line width and rotation velocity, and we verified, through sensitivity tests, that the results are insensitive to the precise values adopted for other parameters (inclination, effective temperature, polar gravity and ω/ω_c).

The Fourier transforms of the observed and model spectra were then compared in order to determine $v \sin i$. We estimate $v \sin i \approx 336$, 318, 310 and 318 $\mathrm{km\,s^{-1}}$ from the Elodie, FEROS, HARPS and UVES spectra, respectively, and adopt $318 \pm 8\,\mathrm{km\,s^{-1}}$ (where the estimated error is dominated by the inter-instrument differences, and accommodates both the small individual uncertainties and the weak sensitivity to other parameters). Comparison of observed and model spectra confirms that this value leads to a satisfactory match, and our result is consistent with the other direct measurements published this century of $300 \pm 20\,\mathrm{km\,s^{-1}}$ (ref. [41]) and $317 \pm 3\,\mathrm{km\,s^{-1}}$ (ref. [5]).

Constraining stellar parameter space. Any modelling of rotating stars (including our polarization calculations) requires a number of stellar parameters as inputs: three to characterize the basic structure (for example effective temperature, mass and polar radius, or surrogates) and two that describe the rotation ($v \sin i$ and inclination i, or surrogates).

The effective temperature of Regulus is such that the bulk of its radiant-energy output is directly observable, and hence the spectral-energy distribution gives a strong constraint on the global effective temperature T_{eff}. Furthermore, the distance to Regulus is precisely determined from *Hipparcos* astrometry[31]: $d = 24.3 \pm 0.2$ pc. Given T_{eff}, the apparent brightness gives the angular size of the star as seen from Earth, whence d yields the stellar radius (polar or equatorial radii r_p, r_{eq}), for any given values of ω/ω_c and i.

Given ω/ω_c and i, the observed $v \sin i$ establishes a value for ω_c, which in turn yields the stellar mass (within the framework of the Roche model; see for example ref. [44]) for the corresponding r_{eq}. Although the line profiles and flux distribution (especially the size of the Balmer jump) potentially offer further leverage on parameters such as polar gravity, g_p, in practice observational uncertainties limit the additional utility of those diagnostics. These principles can therefore be used to determine the effective temperature and polar gravity (along with the stellar mass and radius) from the known distance plus the observed flux distribution and projected equatorial rotation velocity, given values for ω/ω_c and i (which are constrained by the polarization modelling described below).

In practice, we determined temperatures and radii, for specified values of $v \sin i$, ω/ω_c and i, by requiring rotating-star model fluxes to reproduce simultaneously the observed magnitude in the Johnson V band (effective wavelength ~550 nm) and the ultraviolet flux integrated over the range 132.5–194.5 nm. The ultraviolet flux was measured from the archival low-dispersion spectrum SWP 33624 (the same spectrum used in ref. [5]), obtained with the International Ultraviolet Explorer satellite and downloaded from the IUE Final Archive at the Mikulski Archive for Space Telescopes. The required model-atmosphere fluxes and magnitude normalization were taken from ref. [45] and are consistent with those used in the polarization calculations.

The projected equatorial rotation velocity is fairly well determined, leaving ω/ω_c and i as the principal 'free' parameters. Supplementary Fig. 3 shows results of an initial grid, sampled at 0.01 in ω/ω_c and every 5° in i. We calculated additional points on a finer grid (0.005 in ω/ω_c and 2.5° in i) around the region of the best-fitting solution from the polarization analysis. Final numerical results of our analysis of the basic stellar parameters are incorporated into Supplementary Table 8 (where the uncertainties are generated from Monte Carlo simulations, sampling the estimated errors in the input parameters).

Modelling. All our modelling is based on the assumption of a Roche model and uniform rotation. On this basis, the geometry of a rapidly rotating star follows equations[2] that specify how the radius and other properties vary as a function of colatitude (Θ) and rotational velocity expressed as ω/ω_c. Each colatitude has a different value of gravity (g) and local effective temperature ($T_{\rm eff}^{\rm l}$). To represent this variation, we create for each model (where a model is defined by its polar temperature $T_{\rm p}$ and gravity, its ω/ω_c and its gravity-darkening law) a set of 46 ATLAS9 model atmospheres representing the $T_{\rm eff}^{\rm l}$ and $\log g$ of the star at 2° intervals of colatitude from 0 to 90°. The ATLAS9 models use as a basis the Castelli and Kurucz model grid[46] for solar abundances[47].

Polarized radiative transfer. To calculate the polarization of the emission from these models we use a modified version of the SYNSPEC spectral synthesis code of ref. [22]. We have modified the code to do polarized radiative transfer using the Vector Linearized Discrete Ordinate (VLIDORT) code[23], which is a comprehensive implementation of the discrete-ordinate method of radiative transfer.

From the emission, absorption and scattering properties of each layer of the atmosphere available in SYNSPEC, it is straightforward to provide the inputs needed by VLIDORT for each atmospheric layer. We assume that all scattering is described by a Rayleigh scattering matrix, which is appropriate for Thompson scattering from electrons. Our modified version of SYNSPEC outputs the intensity and polarization as a function of viewing angle (μ = cosine of the local zenith angle) and wavelength. SYNSPEC uses a non-uniform wavelength scale to fully sample line structure, which we re-bin to a uniform 0.01-nm spacing for subsequent processing.

To apply the model to a rotating star, we use the geometric model to determine the colatitude Θ and μ as a function of coordinates x, y in the observed image plane for a given inclination i. We divide the observed image into a large number of 'pixels' using a spacing of 0.01 in units of the polar radius of the star. We then interpolate in the grid of models to obtain intensity and polarization for each pixel. We use linear interpolation in Θ and cubic spline interpolation in μ. The polarizations require rotation through an angle ξ as defined in ref. [2] to rotate into a coordinate system defined by the rotation axis of the star.

The results of this process are intensity and polarization values for each pixel, at the full spectral resolution of the model, that can be plotted as an image and vector map as in Fig. 2, or can be integrated over the star to give the total polarization. Because we work in the observed image plane and use a large number of pixels (typically about 40,000), the integration is a simple sum over pixels for each Stokes parameter. To allow a comparison to observation, as in Fig. 4, the integrated intensity and polarization are fed into the bandpass model at the full spectral resolution of the model.

Tests of the modelling. We have tested our polarization version of SYNSPEC by calculating polarization for a number of stellar-atmosphere models that are included in the results of ref. [18]. Supplementary Fig. 4 shows an example for Tlusty[48] models for $T_{\rm eff}$ = 15,000 K and $\log g$ = 2.5 and 3.5 at a wavelength of 400 nm. The polarizations from the two models agree very well. There is a small difference in specific intensity between the results of ref. [18] and those from SYNSPEC/VLIDORT, but our results agree well with intensity from SYNSPEC's standard radiative transfer. This is probably because the calculations of ref. [18] are for continuum only, whereas our models include spectral lines. Similar agreement has been found for other wavelengths and different temperature models.

To test our rotating-star models, we have compared with results reported in ref. [10]. Supplementary Fig. 5 shows a comparison of our modelling with the previous results[10] for B1, B2 and B5 stars with ω/ω_c = 0.95 and i = 90°. In the previous work, the temperature and gravity values used for these models are not specified. However, we found that we could closely match the results with $T_{\rm p}$ = 28,000 K (B1), 23,000 K (B2) and 18,000 K (B5) with a $\log g_{\rm p}$ of 4.07 in all cases. For these models, we used a gravity-darkening law[20] consistent with the original work of ref. [10]. In future work, we plan to examine stars with different spectral types in more detail.

Regulus final parameters. The result of fitting our model grid to the data is shown in Fig. 4. From this, we obtain a best fit in χ^2 and the 1σ confidence region in reduced χ^2 that constitutes the model error. To obtain the final errors, we must also consider the errors in $T_{\rm eff}$ and $\log g_{\rm p}$ due to the uncertainty in the parameters obtained from the literature, particularly the ultraviolet flux, $F_{\rm UV}$ (which we take as 5%), and $v \sin i$. These are shown diagrammatically in the bottom left corner of Supplementary Fig. 3 and are simply added as root mean squares to the model errors to obtain the final uncertainties in $T_{\rm eff}$ and $\log g_{\rm p}$. To calculate the errors in ω/ω_c and i the observational uncertainties in $T_{\rm eff}$ and $\log g_{\rm p}$ must first be transformed into a corresponding change in polarization via an interpolation of the upper two panels of Fig. 4; the change in polarization can then be equated to errors in ω/ω_c and i through the lower two panels of the same figure, and finally added as root mean squares to the model errors. Supplementary Table 8 lists all the parameters adopted and calculated in modelling Regulus, and the final values determined. For other derived physical parameters, given at the bottom of Supplementary Table 8, the errors are propagated from the uncertainties on the model-determined parameters using Monte Carlo methods.

Data availability. All processed data generated during this study are included in this published article (and its Supplementary Information files); the raw data files are available from the corresponding author upon reasonable request. All other data analysed in this work comes from public repositories; where this is the case, the origin of the data is indicated in the text.

Received: 16 June 2017; Accepted: 8 August 2017;
Published online: 18 September 2017

References

1. Chandrasekhar, S. On the radiative equilibrium of a stellar atmosphere. X. *Astrophys. J.* **103**, 351–370 (1946).
2. Harrington, J. P. & Collins, G. W. Intrinsic polarization of rapidly rotating early-type stars. *Astrophys. J.* **151**, 1051–1056 (1968).
3. Che, X. et al. Colder and hotter: interferometric imaging of β Cassiopeiae and α Leonis. *Astrophys. J.* **732**, 68 (2011).
4. Cranmer, S. R. & Owocki, S. P. The effect of oblateness and gravity darkening on the radiation driving winds from rapidly rotating B stars. *Astrophys. J.* **440**, 308–321 (1995).
5. McAlister, H. A. et al. First results from the CHARA array. I. An interferometric and spectroscopic study of the fast rotator α Leonis (Regulus). *Astrophys. J.* **628**, 439–452 (2005).
6. Hiltner, W. A. Polarization of radiation from distant stars by the interstellar medium. *Nature* **163**, 283 (1949).
7. Hall, J. S. Observations of the polarized light from stars. *Science* **109**, 166–167 (1949).
8. Kemp, J. C., Henson, G. D., Barbour, M. S., Kraus, D. J. & Collins, G. W. Discovery of eclipse polarization in Algol. *Astrophys. J. Lett.* **273**, L85–L88 (1983).
9. Collins, G. W. II Intrinsic polarization in nongray atmospheres. *Astrophys. J.* **159**, 583–591 (1970).
10. Sonneborn, G. in *Be Stars* (eds Jaschek M. & Groth H.-G.) 493–496 (Reidel, Dordrecht, 1982).
11. Coyne, G. V. & Kruszewski, A. Wavelength dependence of polarization. XVII. Be-type stars. *Astron. J.* **74**, 528–532 (1969).
12. Clarke, D. *Stellar Polarimetry* (Wiley-VCH, Weinheim, 2010).
13. Porter, J. M. & Rivinius, T. Classical Be stars. *Publ. Astron. Soc. Pacific* **115**, 1153–1170 (2003).
14. Bailey, J. et al. A high-sensitivity polarimeter using a ferro-electric liquid crystal modulator. *Mon. Not. R. Astron. Soc.* **449**, 3064–3073 (2015).
15. Hough, J. H. et al. PlanetPol: a very high sensitivity polarimeter. *Publ. Astron. Soc. Pacific* **118**, 1302–1318 (2006).
16. Wiktorowicz, S. J. & Matthews, K. A high-precision optical polarimeter to measure inclinations of high-mass X-ray binaries. *Publ. Astron. Soc. Pacific* **120**, 1282–1297 (2008).
17. Bailey, J., Lucas, P. W. & Hough, J. H. The linear polarization of nearby bright stars measured at the parts per million level. *Mon. Not. R. Astron. Soc.* **405**, 2570–2578 (2010).
18. Harrington, J. P. in *Polarimetry: From the Sun to Stars and Stellar Environments. Proc. IAU* **10**, 395–400 (2015).
19. Espinosa Lara, F. & Rieutord, M. Gravity darkening in rotating stars. *Astron. Astrophys.* **533**, A43 (2011).
20. von Zeipel, H. The radiative equilibrium of a rotating system of gaseous masses. *Mon. Not. R. Astron. Soc* **84**, 665–683 (1924).
21. Kurucz, R. ATLAS9 Stellar Atmosphere Programs and 2 km/s grid. Kurucz CD-ROM No. 13 (1993).
22. Hubney, I., Stefl, S. & Harmanec, P. How strong is the evidence of superionization and large mass outflows in B/Be stars? *Bull. Astron. Inst. Czech.* **36**, 214–230 (1985).

23. Spurr, R. J. D. VLIDORT: a linearized pseudo-spherical vector discrete ordinate radiative transfer code for forward model and retrieval studies in multilayer scattering media. *J. Quant. Spectrosc. Radiat. Transf.* **102**, 316–342 (2006).
24. Howarth, I. D. & Smith, K. C. Rotational mixing in early-type main-sequence stars. *Mon. Not. R. Astron. Soc.* **327**, 353–368 (2001).
25. Öhman, Y. On the possibility of tracing polarization effects in the rotational profiles of early-type stars. *Astrophys. J.* **104**, 460–462 (1946).
26. Cotton, D. V. et al. The linear polarization of Southern bright stars measured at the parts-per-million level. *Mon. Not. R. Astron. Soc.* **455**, 1607–1628 (2016).
27. Marshall, J. P. et al. Polarization measurements of hot dust stars and the local interstellar medium. *Astrophys. J.* **825**, 124 (2016).
28. Cotton, D. V. et al. The intrinsic and interstellar broad-band linear polarization of nearby FGK dwarfs. *Mon. Not. R. Astron. Soc.* **467**, 873–897 (2017).
29. Thureau, N. D. et al. An unbiased study of debris discs around A-type stars with Herschel. *Mon. Not. R. Astron. Soc.* **445**, 2558–2573 (2014).
30. Frisch, P. C. et al. Following the interstellar magnetic field from the heliosphere into space with polarized starlight. *J. Phys. Conf. Ser.* **767**, 012010 (2016).
31. van Leeuwen, F. Validation of the new Hipparcos reduction. *Astron. Astrophys.* **474**, 653–664 (2007).
32. Serkowski, K., Mathewson, D. S. & Ford, V. L. Wavelength dependence of interstellar polarization and ratio of total to selective extinction. *Astrophys. J.* **196**, 261–290 (1975).
33. Wilking, B. A., Lebofsky, M. J. & Rieke, G. H. The wavelength dependence of interstellar linear polarization: stars with extreme values of λ_{max}. *Astron. J.* **87**, 695–697 (1982).
34. Hiltner, W. A. Interstellar polarization. *Vistas Astron* **2**, 1080–1091 (1956).
35. Slettebak, A., Collins, G. W. II, Parkinson, T. D., Boyce, P. B. & White, N. M. A system of standard stars for rotational velocity determinations. *Astrophys. J. Supp. Ser.* **29**, 137–159 (1975).
36. Zorec, J. & Royer, F. Rotational velocities of A-type stars. IV. Evolution of rotational velocities. *Astron. Astrophys.* **537**, A120 (2012).
37. Dekker, H., D'Odorico, S., Kaufer, A., Delabre, B. & Kotzlowski, H. Design, construction, and performance of UVES, the echelle spectrograph for the UT2 Kueyen Telescope at the ESO Paranal Observatory. *Proc. SPIE* **4008**, 534–545 (2000).
38. Pepe, F. et al. HARPS: a new high-resolution spectrograph for the search of extrasolar planets. *Proc. SPIE* **4008**, 582–592 (2000).
39. Kaufer, A. & Pasquini, L. FEROS: the new fiber-linked echelle spectrograph for the ESO 1.52-m telescope. *Proc. SPIE* **3355**, 844–854 (1998).
40. Baranne, A. et al. ELODIE: a spectrograph for accurate radial velocity measurements. *Astron. Astrophys. Supp. Ser* **119**, 373–390 (1996).
41. Gavrilović, N. & Jankov, S. in *Active OB-Stars: Laboratories for Stellar and Circumstellar Physics. ASP Conf. Ser.* 425–427 (Astronomical Society of the Pacific, 2007).
42. Townsend, R. H. D., Owocki, S. P. & Howarth, I. D. Be-star rotation: how close to critical? *Mon. Not. R. Astron. Soc* **350**, 189–195 (2004).
43. Gray, D. F. *The Observation and Analysis of Stellar Photospheres* 3rd edn (Cambridge Univ. Press, Cambridge, 2005).
44. Howarth, I. D. & Morello, G. Rapid rotators revisited: absolute dimensions of KOI-13. *Mon. Not. R. Astron. Soc* **470**, 932–939 (2017).
45. Howarth, I. D. New limb-darkening coefficients and synthetic photometry for model-atmosphere grids at Galactic, LMC, and SMC abundances. *Mon. Not. R. Astron. Soc.* **413**, 1515–1523 (2011).
46. Castelli, F. & Kurucz, R. New grids of ATLAS9 model atmospheres. Preprint at http://arXiv.org/abs/astroph/0405087 (2004).
47. Grevesse, N. & Sauval, A. J. Standard solar composition. *Space Sci. Rev* **85**, 161–174 (1998).
48. Hubeny, I. & Lanz, T. Non-LTE line-blanketed model atmospheres of hot stars. 1: Hybrid complete linearization/accelerated lambda iteration method. *Astrophys. J.* **439**, 875–904 (1995).

Acknowledgements

The work was supported by the Australian Research Council through Discovery Project grants DP140100121 and DP160103231. We thank D. Opitz, J. Sturges and the staff at the AAT for their assistance in making the HIPPI observations. We thank R. Spurr of RT Solutions for providing the VLIDORT software.

Author contributions

J.B., D.V.C., L.K.-C., K.B., P.W.L. and J.H.H. drafted the initial proposals to observe Regulus with HIPPI, following an extended discussion of the PlanetPol results dating back to 2010 that included I.D.H., J.H.H., J.B. and P.W.L. All authors contributed to the discussion and drafting of the final manuscript. The HIPPI observations were carried out and directed by J.B., D.V.C., L.K.-C. and K.B. In addition, the following authors made specific contributions to the work: D.V.C. contributed the initial data analysis, telescope polarization subtraction, stellar atmosphere modelling, interstellar subtraction, model comparison to data, and other calculations including the position angle calculation and the calculations related to Regulus' companions. J.B. contributed the polarized radiative transfer modelling and verification, gravity-darkening calculations and PlanetPol bandpass model calculations and code. I.D.H. contributed rotational velocity calculations, the knowledge and calculations needed to constrain parameter space, and other miscellaneous calculations. K.B. contributed HIPPI bandpass model calculations and code, and research on Regulus' companions. P.W.L. contributed details of the PlanetPol observations not otherwise available.

Competing interests

The authors declare no competing financial interests.

Additional information

Supplementary information is available for this paper at doi:10.1038/s41550-017-0238-6.

Correspondence and requests for materials should be addressed to D.V.C.